

HYPERDIFFUSION AS A MECHANISM FOR SOLAR CORONAL HEATING

A. A. VAN BALLEGOOIJEN AND S. R. CRANMER

Harvard-Smithsonian Center for Astrophysics, 60 Garden Street, Cambridge, MA 02138, USA

Draft version October 27, 2018

ABSTRACT

A theory for the heating of coronal magnetic flux ropes is developed. The dissipated magnetic energy has two distinct contributions: (1) energy injected into the corona as a result of granule-scale, random footpoint motions, and (2) energy from the large-scale, nonpotential magnetic field of the flux rope. The second type of dissipation can be described in term of hyperdiffusion, a type of magnetic diffusion in which the helicity of the mean magnetic field is conserved. The associated heating rate depends on the gradient of the torsion parameter of the mean magnetic field. A simple model of an active region containing a coronal flux rope is constructed. We find that the temperature and density on the axis of the flux rope are lower than in the local surroundings, consistent with observations of coronal cavities. The model requires that the magnetic field in the flux rope is stochastic in nature, with a perpendicular length scale of the magnetic fluctuations of order 1000 km.

Subject headings: MHD — magnetic fields — turbulence — Sun: corona — Sun: magnetic fields

1. INTRODUCTION

In this paper we consider the heating of the solar corona in regions where the large-scale magnetic field deviates significantly from a (current-free) potential field. Evidence for such nonpotential structures comes from a variety of sources. Measurements of photospheric vector fields in active regions often show deviations from the potential field (e.g., Gary et al. 1987; Pevtsov et al. 1995, 1997; Leka et al. 1996). X-ray observations show *sigmoids*, which are bright S-shaped or inverse S-shaped structures inside or between active regions (e.g., Acton et al. 1992; Rust & Kumar 1996; Canfield et al. 1999; Sterling et al. 2000; Gibson 2002). These sigmoids contain coronal loops that are highly sheared with respect to the photospheric polarity inversion line (PIL), and are often associated with H α filaments (e.g., Manoharan et al. 1996; Pevtsov 2002; Gibson & Fan 2006a). Schmieder et al. (1996) proposed a differential magnetic shear model in which the degree of shear decreases with height in the observed active region. Schrijver et al. (2005) studied the nonpotentiality of active regions using extreme-ultraviolet (EUV) images from the *Transition Region and Coronal Explorer* (TRACE). They found that significant nonpotentiality occurs when new magnetic flux has recently emerged into the corona, or when rapidly evolving, opposite polarity flux concentrations are in close contact. Mandrini et al. (2000) tested various models of coronal heating using potential, linear force-free, and magnetostatic models. Of course, nonpotential magnetic fields also play an important role in solar flares and coronal mass ejections (see Fan & Gibson 2007, and references therein).

The nonpotential structures in the corona have been modeled as *flux ropes* in which the field lines twist about an axial field line (e.g., Rust & Kumar 1994; Low & Hundhausen 1995; Aulanier & Démoulin 1998; Titov & Démoulin 1999; Amari et al. 2003; Magara & Longcope 2001; Kliem et al. 2004; Kusano 2005; Aulanier et al. 2005; Gibson et al. 2006a). The presence of a coronal flux rope implies the existence of electric currents that pass through the photosphere and into the corona. The corona of an active region is a magnetically dominated plasma. Therefore, except during a flare or eruption, the corona is nearly force

free, $\nabla \times \mathbf{B} \approx \alpha \mathbf{B}$, where $\mathbf{B}(\mathbf{r})$ is the magnetic field and $\alpha(\mathbf{r})$ is the so-called torsion parameter. A magnetic field with this property is called a nonlinear force-free field (NLFFF). Many authors have developed NLFFF models of active regions, either by extrapolating photospheric vector fields into the corona (e.g., Wheatland et al. 2000; Bleybel et al. 2002; Régnier et al. 2002; Wiegmann 2004; Valori et al. 2005; Wheatland 2006; Régnier & Priest 2007), or using a flux rope insertion method (van Ballegoijen 2004; Bobra et al. 2008).

Active regions exhibit transient brightenings at EUV and soft X-ray wavelengths on time scales of a few minutes (e.g., Shimizu et al. 1992; Shimizu 1995; Porter et al. 1995; Berghmans & Clette 1999; Berghmans et al. 2001). These single- or multi-loop brightenings are thought to be due to the release of magnetic energy by small reconnection events in the complex coronal field of an active region. This may be a two-step process: magnetic energy may first be converted into kinetic energy of reconnection outflows, waves or energetic particles, and then be converted into thermal energy of the plasma (Longcope 2004). It seems likely that X-ray sigmoids are also heated by such reconnection events, with many events occurring simultaneously at different sites within the sigmoid. The events may occur so frequently that the coronal plasma does not have time to cool significantly between heating events, keeping the plasma at temperatures of 3-5 MK (e.g., Klimchuk & Porter 1995; Cargill & Klimchuk 2004). This would explain why sigmoids generally do not show up in EUV spectral lines formed at 1-1.5 MK.

What is the origin of the energy released in small reconnection events? One possibility is that the energy is injected into the corona by small-scale random footpoint motions, which lead to twisting and braiding of coronal field lines (e.g., Parker 1972, 1988). However, in the highly sheared magnetic field of a sigmoid there is another possibility, namely, that the energy for coronal heating is derived from the energy of the flux rope itself. In this case the energy is already stored in the corona and does not need to be injected at the photospheric footpoints. Generally, a large amount of free energy is available in the coronal flux rope ($\sim 10^{32}$ erg), sufficient to explain both the heating of the coronal plasma and the occurrence of flares and coronal mass ejections.

The second scenario leads us to propose a new theory for

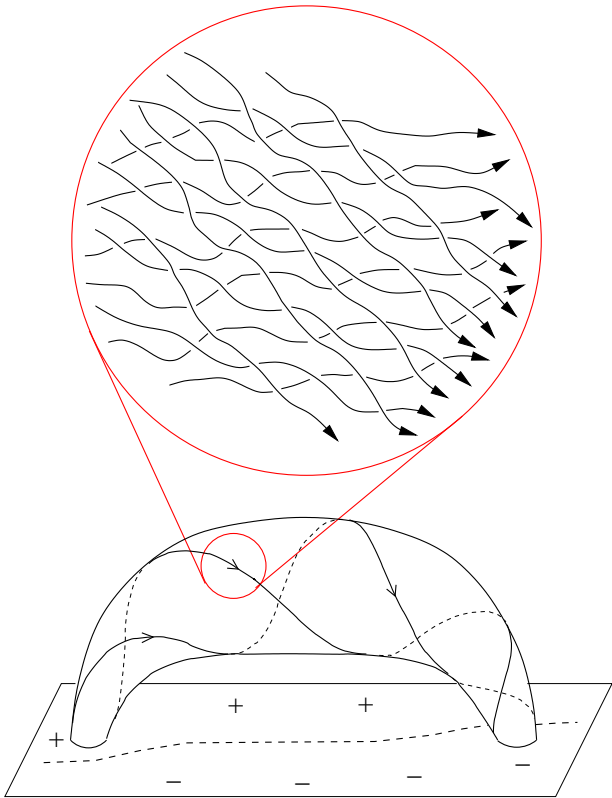


FIG. 1.— Stochastic magnetic fields in a coronal flux rope.

the heating of coronal flux ropes. The basic ideas are illustrated in Figure 1. The lower part of the figure shows a flux rope in the low corona. Inside the flux rope is a magnetic field that runs more or less parallel to the flux rope axis. The flux rope is held down by an overlying coronal arcade (not shown), which has a magnetic field that runs perpendicular to the flux rope axis. Hence, going from the inside to the outside of the flux rope the direction of the mean magnetic field rotates through an angle of about 90 degrees. The upper part of the figure shows the fine-scale structure of the magnetic field at the boundary between the flux rope and its surroundings. The magnetic field has both mean and fluctuating components, as indicated by the wiggles in the field lines. The total magnetic field $\mathbf{B}(\mathbf{r})$ is assumed to be stochastic in nature (Lazarian & Vishniac 1999). The magnetic fluctuations are assumed to be produced by some unspecified MHD process that ultimately derives its energy from the free magnetic energy of the coronal flux rope. Strauss (1988) proposed that turbulent fluctuations could be produced by tearing modes in coronal current sheets, but the present paper does not depend on that particular mechanism. We only assume that reconnection occurs intermittently at many sites in the stochastic field. The reconnection events produce outflows and energetic particles that ultimately result in heating of the coronal plasma.

The above process is an example of a “dynamo” process because it involves turbulent diffusion of the mean magnetic field of the coronal flux rope. Dynamo activity, defined as the amplification and/or maintenance of large-scale magnetic fields, occurs in many astrophysical and laboratory plasmas, and magnetic helicity evolution plays an important role in such activity (e.g., Blackman & Ji 2006; Subramanian & Brandenburg 2006). Boozer (1986) and Bhattacharjee & Hameiri (1986) considered turbulence in low- β plasmas, and proposed that the evolution of the

mean magnetic field can be described in term of *hyperdiffusion*, a type of magnetic diffusion in which the magnetic helicity of the mean field is conserved. Strauss (1988) proposed that tearing modes can produce turbulence in three-dimensional sheared magnetic fields, and showed that such turbulence causes hyperdiffusion, which may explain both fast reconnection in solar flares and the heating of the solar corona. Bhattacharjee & Yuan (1995) considered the constraints on the dynamo mechanism from helicity conservation and the back-reaction of the magnetic field on plasma dynamics. They showed that the results of kinematic dynamo theory are strongly modified by the production of hyperdiffusion in the mean field equation. Hyperdiffusion has also been included in models for decaying active regions (van Ballegoijen & Mackay 2007).

In the present paper we consider the plasma heating associated with hyperdiffusion. At present, it is unclear to what extent stochastic effects dominate the solar magnetic field. Our purpose here is not to develop a complete theory of such fields, but rather to determine some of the observable consequences of their existence. Therefore, more detailed questions, such as how the stochastic field is produced and the nature of the MHD instabilities, will remain unanswered. The main goal is to demonstrate that the existence of stochastic fields is consistent with existing observations of coronal heating in active regions.

2. THEORY OF HYPERDIFFUSION

The theory of hyperdiffusion was first proposed by Boozer (1986) and Bhattacharjee & Hameiri (1986), and further developed by Strauss (1988), Bhattacharjee & Yuan (1995), Vishniac & Cho (2001) and others. In this section we summarize the results of these analyses as they apply to the solar corona, i.e., when the plasma is magnetically dominated. The total magnetic field $\mathbf{B}(\mathbf{r}, t)$ is a sum of mean and fluctuating components, and is described in terms of the vector potential $\mathbf{A}(\mathbf{r}, t)$, where $\mathbf{B} \equiv \nabla \times \mathbf{A}$. The evolution equation for the vector potential is

$$\frac{\partial \mathbf{A}}{\partial t} = -c\mathbf{E} - \nabla\Phi, \quad (1)$$

where $\mathbf{E}(\mathbf{r}, t)$ is the electric field, $\Phi(\mathbf{r}, t)$ is the scalar potential, and c is the speed of light. Inserting Ohm’s law and Ampere’s law, we obtain

$$\frac{\partial \mathbf{A}}{\partial t} = \mathbf{v} \times \mathbf{B} - \eta \nabla \times \mathbf{B} - \nabla\Phi, \quad (2)$$

where $\mathbf{v}(\mathbf{r}, t)$ is the plasma velocity, and η is the Ohmic diffusivity. We assume that $\eta \ll L^2/\tau$, where L is the system size and τ is the time scale for the evolution of the mean magnetic field. Then reconnection occurs only in highly localized regions (e.g., current sheets) that make up only a small fraction of the volume. Following Vishniac & Cho (2001), we use the Coulomb gauge, $\nabla \cdot \mathbf{A} = 0$, so that the scalar potential is given by

$$\nabla^2\Phi = \nabla \cdot (\mathbf{v} \times \mathbf{B} - \eta \nabla \times \mathbf{B}). \quad (3)$$

The magnetic helicity equation follows from equation (2):

$$\frac{\partial}{\partial t} (\mathbf{A} \cdot \mathbf{B}) + \nabla \cdot \mathcal{H} = -2\eta \mathbf{B} \cdot \nabla \times \mathbf{B}, \quad (4)$$

where $(\mathbf{A} \cdot \mathbf{B})$ is the helicity density, and $\mathcal{H}(\mathbf{r}, t)$ is the helicity flux:

$$\begin{aligned} \mathcal{H} &\equiv \mathbf{A} \times (\mathbf{v} \times \mathbf{B} - \eta \nabla \times \mathbf{B} + \nabla\Phi) \\ &= \mathbf{A} \times (-c\mathbf{E} + \nabla\Phi). \end{aligned} \quad (5)$$

Berger (1984) has shown that in the limit $\eta \ll L^2/\tau$ the right-hand side of equation (4) can be neglected, so this equation describes the conservation of magnetic helicity. The relative magnetic helicity is defined by $H_R \equiv \int [\mathbf{A} \cdot \mathbf{B} - \mathbf{A}_p \cdot \mathbf{B}_p] dV$, where subscript p refers to the potential field, and the integration includes the coronal and subsurface regions (see Berger & Field 1984). Therefore, in the limit $\eta \ll L^2/\tau$, if no helicity is injected into the corona at the photosphere or ejected into the heliosphere, H_R is constant in time.

Let $\mathbf{B}_0(\mathbf{r}, t)$ be the mean magnetic field smoothed over some intermediate spatial scale ℓ , and let $\mathbf{B}_1(\mathbf{r}, t)$ be the fluctuating field on scales less than ℓ . Similar decompositions are made for other physical quantities. Applying the smoothing operator to equations (1) and (2), we obtain:

$$\frac{\partial \mathbf{A}_0}{\partial t} = -c\mathbf{E}_0 - \nabla \Phi_0 \approx \mathbf{v}'_0 \times \mathbf{B}_0 + \mathcal{E}_0 - \nabla \Phi_0, \quad (6)$$

where \mathbf{A}_0 , Φ_0 , \mathbf{E}_0 and \mathbf{v}'_0 are the mean vector potential, scalar potential, electric field and plasma velocity, and $\mathcal{E}_0 \equiv \langle \mathbf{v}_1 \times \mathbf{B}_1 \rangle$ is the ‘‘mean electromotive force’’ describing the effect of the fluctuations on the mean magnetic field (Steenbeck et al. 1966). Here we neglected the Ohmic diffusion of the mean field. The helicity equation for the mean magnetic field can be derived from equation (6):

$$\frac{\partial}{\partial t} (\mathbf{A}_0 \cdot \mathbf{B}_0) + \nabla \cdot [\mathbf{A}_0 \times (\mathbf{v}'_0 \times \mathbf{B}_0 + \mathcal{E}_0 + \nabla \Phi_0)] = 2\mathcal{E}_0 \cdot \mathbf{B}_0. \quad (7)$$

On the other hand, applying the smoothing operator directly to equation (4) with $\eta \approx 0$, we obtain:

$$\frac{\partial}{\partial t} (\langle \mathbf{A} \cdot \mathbf{B} \rangle) + \nabla \cdot [\mathbf{A}_0 \times (\mathbf{v}'_0 \times \mathbf{B}_0 + \mathcal{E}_0 + \nabla \Phi_0) + \mathcal{H}_0] = 0, \quad (8)$$

where \mathcal{H}_0 is the contribution of the fluctuations to the helicity flux:

$$\mathcal{H}_0 \equiv \langle \mathbf{A}_1 \times (-c\mathbf{E}_1 + \nabla \Phi_1) \rangle. \quad (9)$$

We assume that the large-scale structures dominate the helicity budget, so that the helicity of the total field can be approximated by the helicity of the mean field, $\langle \mathbf{A} \cdot \mathbf{B} \rangle \approx \mathbf{A}_0 \cdot \mathbf{B}_0$ (Boozer 1986; Bhattacharjee & Hameiri 1986; Vishniac & Cho 2001). Subtracting equation (7) from equation (8) yields the following relationship between \mathcal{E}_0 and \mathcal{H}_0 :

$$2\mathcal{E}_0 \cdot \mathbf{B}_0 = -\nabla \cdot \mathcal{H}_0. \quad (10)$$

The electromotive force can be written as a sum of components parallel and perpendicular to the mean magnetic field, $\mathcal{E}_0 = \mathcal{E}_{0,\parallel} + \mathcal{E}_{0,\perp}$. The parallel component is given by equation (10), and the perpendicular component can be written in terms of a transport velocity \mathbf{u}_0 , which is defined by $\mathbf{u}_0 \equiv (\mathbf{B}_0 \times \mathcal{E}_{0,\perp})/B_0^2$. Then the electromotive force is given by

$$\mathcal{E}_0 = \mathbf{u}_0 \times \mathbf{B}_0 - \frac{\nabla \cdot \mathcal{H}_0}{2B_0^2} \mathbf{B}_0. \quad (11)$$

We assume that the magnetic field evolves slowly in response to hyperdiffusion and changes in the boundary conditions. Furthermore, we assume that the magnetic pressure is much larger than the plasma pressure, so that the mean magnetic field evolves through a series of force-free equilibrium states, $(\nabla \times \mathbf{B}_0) \times \mathbf{B}_0 \approx 0$. The force-free condition can also be written as

$$\nabla \times \mathbf{B}_0 = \alpha_0 \mathbf{B}_0, \quad (12)$$

where α_0 is the torsion parameter of the mean field. For a linear force free field ($\alpha_0 = \text{constant}$) the helicity flux \mathcal{H}_0 should

vanish because there is no magnetic free energy available to drive the magnetic fluctuations. Therefore, following Boozer (1986) and Bhattacharjee & Hameiri (1986) we assume that \mathcal{H}_0 is proportional to the gradient of α_0 :

$$\mathcal{H}_0 = -2\eta_4 B_0^2 \nabla \alpha_0, \quad (13)$$

where η_4 is the so-called hyperdiffusivity. Inserting expression (13) into equations (11) and (6) yields the following diffusion equation for the mean magnetic field:

$$\frac{\partial \mathbf{A}_0}{\partial t} = \mathbf{v}_0 \times \mathbf{B}_0 + \frac{\mathbf{B}_0}{B_0^2} \nabla \cdot (\eta_4 B_0^2 \nabla \alpha_0) - \nabla \Phi_0, \quad (14)$$

where $\mathbf{v}_0 \equiv \mathbf{v}'_0 + \mathbf{u}_0$ is the total transport velocity. The second term on the right-hand side of equation (14) describes the effect of the magnetic fluctuations in diffusing the mean magnetic field. The effect is such that the magnetic helicity of the system is conserved. Hyperdiffusion describes the tendency of the magnetic field to relax to a state of constant α_0 (Taylor 1974). The heating of the coronal plasma resulting from Taylor relaxation was first modeled by Heyvaerts & Priest (1984).

The energy equation for the mean magnetic field can be derived from equations (6), (11) and (12):

$$\frac{\partial}{\partial t} \left(\frac{B_0^2}{8\pi} \right) + \nabla \cdot \left(\frac{c}{4\pi} \mathbf{E}_0 \times \mathbf{B}_0 \right) = -\frac{c}{4\pi} \mathbf{E}_0 \cdot (\nabla \times \mathbf{B}_0) = -\frac{\alpha_0}{8\pi} \nabla \cdot \mathcal{H}_0, \quad (15)$$

and inserting equation (13) we can write

$$\frac{\partial}{\partial t} \left(\frac{B_0^2}{8\pi} \right) + \nabla \cdot \left(\frac{B_0^2}{4\pi} \mathbf{v}_{0,\perp} - \eta_4 \frac{B_0^2}{4\pi} \alpha_0 \nabla \alpha_0 \right) = -\eta_4 \frac{B_0^2}{4\pi} |\nabla \alpha_0|^2. \quad (16)$$

where $\mathbf{v}_{0,\perp} \equiv \mathbf{v}'_{0,\perp} + \mathbf{u}_0$ is the total transport velocity. The quantity on the RHS of equation (16) is negative and can be interpreted as the rate at which mean magnetic energy is converted into heat (Boozer 1986; Bhattacharjee & Hameiri 1986). Assuming there is no inflow of energy at the boundaries, the total magnetic energy decreases monotonically with time:

$$\frac{d}{dt} \left(\int \frac{B_0^2}{8\pi} dV \right) = - \int \eta_4 \frac{B_0^2}{4\pi} |\nabla \alpha_0|^2 dV < 0. \quad (17)$$

3. HELICITY FLUX IN STOCHASTIC MAGNETIC FIELDS

The above theory predicts a particular form of the mean-field diffusion equation, but does not explain why the helicity flux \mathcal{H}_0 is proportional to $\nabla \alpha_0$, nor does it predict the value of the hyperdiffusivity $\eta_4(\mathbf{r}, t)$ contained in equation (13). To estimate this quantity, a detailed understanding of the processes that drive the magnetic fluctuations would be required. Strauss (1988) assumed the fluctuations are driven by tearing mode instability, but in the present paper we make no assumption about the nature of the instability. We only assume that (1) the driving process results in stochastic magnetic field lines (Lazarian & Vishniac 1999), as illustrated in Fig. 1; (2) reconnection occurs intermittently at many sites within this stochastic field; (3) the reconnection events result in Alfvénic perturbations that travel along the stochastic field lines until they are damped as a result of turbulent cascade. Therefore, the magnetic field is not completely force free. In a non-force-free field, the magnetic torsion parameter α can be defined as $\alpha \equiv (\mathbf{B} \cdot \nabla \times \mathbf{B})/B^2$, and we assume that this quantity varies in a time-dependent way along the field lines. The topology of the field is continually changing as a result of the reconnection processes, with new magnetic connections being formed and other connections being severed.

Consider a small volume near the edge of the coronal flux rope where the mean torsion $\alpha_0(\mathbf{r})$ can be approximated as a linear function of position. Let z be the coordinate perpendicular to the surfaces of constant α_0 (we assume $d\alpha_0/dz > 0$). We assume that at time $t = 0$ magnetic reconnection occurs at some localized site, creating a new magnetic connection between two neighboring surfaces $z = \text{constant}$. Let P_1 and P_2 be two points on the newly formed field line, such that P_1 is located on $z = z_1$ and P_2 is located on $z = z_2 > z_1$. The displacement Δs between these two points as measured along the field line is assumed to be much larger than the distance Δz between the two surfaces. The displacements are given by

$$\Delta z \sim \lambda_{\perp}, \quad \Delta s \sim \lambda_{\parallel}, \quad (18)$$

where λ_{\parallel} and λ_{\perp} are the parallel- and perpendicular length scales of the turbulent motions (relative to the mean magnetic field). The torsion parameters $\alpha(P_1)$ and $\alpha(P_2)$ at the two points differ by an amount

$$\Delta\alpha \equiv \alpha(P_2) - \alpha(P_1) \approx \alpha_0(z_2) - \alpha_0(z_1) \approx \Delta z \frac{d\alpha_0}{dz}. \quad (19)$$

We assume that this difference in torsion results in the launch of Alfvén waves that travel in both directions along the newly formed field line. In Appendix A we show that these waves carry a certain amount of magnetic helicity. The net helicity flux due to the waves can be estimated by inserting expression (19) into equation (A14):

$$\mathcal{H}_{\parallel} \approx -f_0 \lambda_{\perp}^2 v_A B_0^2 \Delta z \frac{d\alpha_0}{dz}, \quad (20)$$

where v_A is the Alfvén speed, and we assume that the radius R of the newly formed flux tube is determined by the outer scale of the turbulence, $R \approx \lambda_{\perp}$. The quantity f_0 is a dimensionless constant, and we estimate it to be rather small, $f_0 \approx 0.01$ (see Appendix). The z -component of the helicity flux is

$$\mathcal{H}_{0,z} \approx \mathcal{H}_{\parallel} \frac{\Delta z}{\Delta s} \approx -f_0 \lambda_{\perp}^4 \lambda_{\parallel}^{-1} v_A B_0^2 \frac{d\alpha_0}{dz}, \quad (21)$$

where we take into account the angle of the field lines with respect to the z -direction, and we use equations (20) and (18). This shows that the helicity flux \mathcal{H}_0 due to the fluctuations is proportional to the local gradient of α_0 , as assumed in equation (13). Furthermore, we obtain the following estimate for the hyperdiffusivity:

$$\eta_4 \approx f_0 \lambda_{\perp}^4 \lambda_{\parallel}^{-1} v_A. \quad (22)$$

Note that η_4 depends strongly on the perpendicular length scale of the turbulent motions associated with the reconnection in the stochastic magnetic field.

4. CORONAL HEATING

The coronal magnetic field is anchored in the photosphere where the field is highly fragmented (Stenflo 1989). The photospheric field consists of vertically oriented, kilo-Gauss *flux tubes* separated by nearly field-free plasma. These flux elements are continually buffeted by convective flows on the scale of the solar granulation, which results in random twisting of the flux tubes and a random walk of the flux elements over the solar surface (e.g., Berger & Title 1996; Nisenson et al. 2003). Both types of motions cause disturbances that propagate upward along the field lines in the form of Alfvén waves (e.g., Cranmer & van Ballegoijen 2005). In coronal loops, such disturbances produce small-scale twisting

and braiding of the coronal field lines and associated field-aligned electric currents (Parker 1972). Schrijver (2007) argues that the observed widths of coronal loops are determined by these footpoint motions. The random walk of the footpoints is predicted to drive a cascade of magnetic energy from large to small spatial scales (van Ballegoijen 1985, 1986, 1988; Craig & Sneyd 2005). The existence of such a cascade is confirmed by results from 3D numerical simulations of the Parker problem with incompressible boundary flows (e.g., Mikić et al. 1989; Hendrix & van Hoven 1996; Hendrix et al. 1996; Galsgaard & Nordlund 1996; Rappazzo et al. 2007). However, the twisting motions of the flux tubes may be more important than the lateral motions, as the twist velocity is amplified by the expansion of the flux tubes (van Ballegoijen 1986; Mandrini et al. 2000). At the smallest scales in the corona, impulsive reconnection events (“nanoflares”) play an important role in the release of the magnetic energy (Parker 1988; Lu & Hamilton 1991). The actual dissipation may be a multi-step process involving reconnection outflows, waves, and energetic particles (Longcope 2004). Gudiksen & Nordlund (2005) have modeled the coronal heating that ultimately results from granule-scale footpoint motions.

In this paper we assume that the coronal heating rate ϵ has contributions from two different sources: (1) dissipation of energy that was directly injected into the corona by granule-scale footpoint motions, as described above; (2) dissipation of energy from a large-scale coronal flux rope via the process of hyperdiffusion. The former uses energy propagated upward along the field lines, while the latter draws its energy from large-scale magnetic shear already present in the corona. The direct contribution to the heating is approximately given by

$$\epsilon_{\text{direct}}(s) \approx \tilde{q} \frac{B_0^2(s) u^2(s) \tau_{\text{ph}}}{4\pi L^2}, \quad (23)$$

where s is the position along the coronal loop, $\epsilon_{\text{direct}}(s)$ is the heating rate per unit volume, $B_0(s)$ is the magnetic field strength, $u(s)$ is the velocity of the perpendicular motions, τ_{ph} is the correlation time of the photospheric motions, L is the loop length, and $\tilde{q} \approx 3$. This expression is a generalization of equation (61) in van Ballegoijen (1986), using a magnetic Reynolds number $R_m \sim 10^{10}$. Equation (23) assumes that the Alfvén-travel time along the coronal loop is short compared to the correlation time, $L/v_A < \tau_{\text{ph}}$. The perpendicular velocity is given by

$$u(s) \approx u_{\text{ph}} \sqrt{\frac{B_{\text{ph}}}{B_0(s)}}, \quad (24)$$

where u_{ph} is the root-mean-square velocity in the photosphere, B_{ph} is the photospheric field strength, and we assume that the magnetic flux associated with the perturbations is constant along the field lines from the base of the photosphere into the corona. Combining the above equations, the direct heating rate is

$$\epsilon_{\text{direct}}(s) \approx \tilde{q} \frac{B_{\text{ph}} u_{\text{ph}}^2 \tau_{\text{ph}}}{4\pi L^2} B_0(s), \quad (25)$$

similar to equation (67) of van Ballegoijen (1986). In the present paper we use $B_{\text{ph}} = 1$ kG, $u_{\text{ph}} = 0.35$ km s⁻¹, and $\tau_{\text{ph}} = 600$ s, which yields a photospheric diffusion constant $D = 92$ km² s⁻¹ [see equation (62) of van Ballegoijen (1986)], consistent with the observed dispersal coefficient that characterizes the granular random walk up to several hours (Hagenaar et al. 1997).

The heating rate due to hyperdiffusion follows from equations (16) and (22):

$$\epsilon_{\text{hyper}}(s) \equiv \eta_4 \frac{B_0^2}{4\pi} |\nabla \alpha_0|^2 \approx f_0 \frac{B_0^2(s) \lambda_{\perp}^4(s)}{4\pi L} v_A(s) |\nabla \alpha_0|^2, \quad (26)$$

where we assume that the parallel length scale of the fluctuations is determined by the loop length, $\lambda_{\parallel} \sim L$. The perpendicular length scale $\lambda_{\perp}(s)$ of the turbulence is assumed to vary along the field lines in a manner consistent with magnetic flux conservation:

$$\lambda_{\perp}(s) \approx \lambda_{\text{turb}} \sqrt{\frac{B_{\text{ph}}}{B_0(s)}}, \quad (27)$$

where λ_{turb} is the corresponding length scale in the photosphere. However, the turbulence is not driven by the foot-point motions, therefore λ_{turb} does not necessarily reflect any property of the photospheric velocity field. We cannot provide a more detailed expression for λ_{turb} because the nature of the physical processes that produce the stochastic field are still unclear; instead, we treat λ_{turb} as a free parameter of the model. Combining the above expressions, we find

$$\epsilon_{\text{hyper}}(s) \approx f_0 \frac{B_{\text{ph}}^2 \lambda_{\text{turb}}^4}{4\pi L} v_A(s) |\nabla \alpha_0|^2, \quad (28)$$

The total heating rate is assumed to be the sum of expressions (25) and (28):

$$\epsilon(s) = \epsilon_{\text{direct}}(s) + \epsilon_{\text{hyper}}(s). \quad (29)$$

In the next section we use these expressions to compute the coronal temperature and density, which provides a link to solar observations.

5. ACTIVE REGION MODEL

Bobra et al. (2008) developed empirical models for NLFFFs in two active regions observed with TRACE. Our initial goal was to compute temperatures and densities for these models. However, we found that small deviations from the force-free condition can cause significant errors in the distribution of $\nabla \alpha_0$ along the field lines, so that the heating rate $\epsilon_{\text{hyper}}(s)$ cannot yet be accurately computed from such empirical models. Therefore, in the present paper we apply the above expressions for the heating rate to a semi-analytic model of an active region. The model describes the *mean* magnetic field $\mathbf{B}_0(\mathbf{r})$ in the corona; fluctuating fields are not modeled, nor do we consider the evolution of the mean field.

The NLFFF model is constructed as follows. We use a Cartesian coordinate system (x, y, z) with z being the height above the coronal base. Following Titov & Démoulin (1999), we assume that the magnetic field has cylindrical symmetry with respect to an axis that lies horizontally below the coronal base at $y = 0$, $z = -R$. Let (r, ϕ, x) be a cylindrical coordinate system with r the distance from the cylinder axis and x the distance along the axis. We consider a finite domain $r = [R, R_m]$ and $x = [-x_m, x_m]$, where the inner radius of the domain is given by R , and $x_m \gg R$. We initially use dimensionless units such that $R = 1$. The force free field is written as:

$$B_{0,r} = -\frac{1}{r} \frac{\partial A}{\partial x}, \quad B_{0,x} = \frac{1}{r} \frac{\partial A}{\partial r}, \quad B_{0,\phi} = \frac{B(A)}{r}, \quad (30)$$

where $A(r, x)$ is the flux function, and $B(A)$ describes the azimuthal component of the field. The flux function satisfies the following non-linear equation:

$$r \frac{\partial}{\partial r} \left(\frac{1}{r} \frac{\partial A}{\partial r} \right) + \frac{\partial^2 A}{\partial x^2} + \alpha_0(A) B(A) = 0, \quad (31)$$

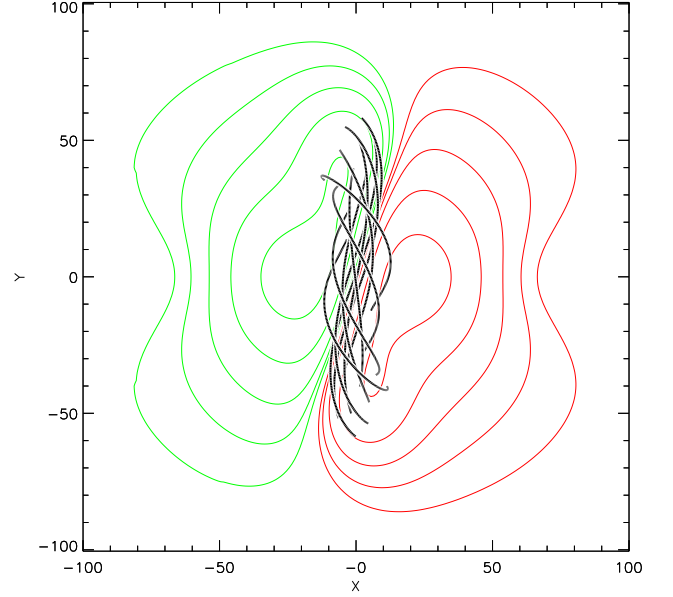


FIG. 2.— Non-linear force-free field model of an active region containing a magnetic flux rope. The contours show the flux distribution on the photosphere (*red*: positive flux; *green*: negative flux). The black lines show selected field lines in the flux rope.

where $\alpha_0(A) \equiv dB/dA$. In this paper we use boundary conditions such that $A(1, x) = 0.8 \exp(-x^2)$ at the inner boundary, and $A = 0$ at the outer boundaries. The azimuthal field is given by

$$B(A) = \beta [1 - \exp(-A^5)]. \quad (32)$$

where β is a parameter describing the magnitude of the azimuthal field. Equation (31) is solved using a relaxation technique. In essence, we solve the following time-dependent equation:

$$\frac{\partial A}{\partial t} = D \left[r \frac{\partial}{\partial r} \left(\frac{1}{r} \frac{\partial A}{\partial r} \right) + \frac{\partial^2 A}{\partial x^2} + \alpha_0(A) B(A) \right], \quad (33)$$

until a stationary solution $A(r, x)$ is obtained (here D is a dimensionless diffusion constant). In each time step, β is adjusted such that the total azimuthal current has a fixed value, $\int \int \alpha_0 B \, dx dz = 2.5$. Once a stationary solution is obtained, the spatial scale is changed to $R = 30$ Mm, and the magnetic field is rescaled by a factor 100, producing a maximum value of $|B_{0,\phi}|$ of 55 G. The quantities $B_{0,r}$, $B_{0,x}$ and $B_{0,\phi}$ are computed on a grid of 200×200 points in the (r, x) plane. The magnetic vector $\mathbf{B}_0(x, y, z)$ in the cartesian frame can then be found by evaluating these quantities at $r = \sqrt{y^2 + (R+z)^2}$. Figure 2 shows the magnetic flux distribution at the coronal base ($z = 0$) and selected field lines in the flux rope. The stability of the Titov & Démoulin (1999) model has been considered by Török et al. (2004). They find that the $m = 1$ kink mode is stable provided the average twist in the flux rope is less than 3.5π . This condition is satisfied in the present case, so we assume that the field shown in Fig. 2 is stable.

The NLFFF model provides the spatial distribution of $\alpha_0(\mathbf{r})$, which is needed to compute the heating rate ϵ . We trace a large number of field lines that cross the vertical plane $y = 0$, and solve the energy balance equation for each field line. We use a modified version of the iterative method described by Schrijver & van Ballegooijen (2005). The code assumes steady-state heating, and includes thermal conduction and optically thin radiative losses. The contribution to the heating from hyperdiffusion is determined from equation (28) with

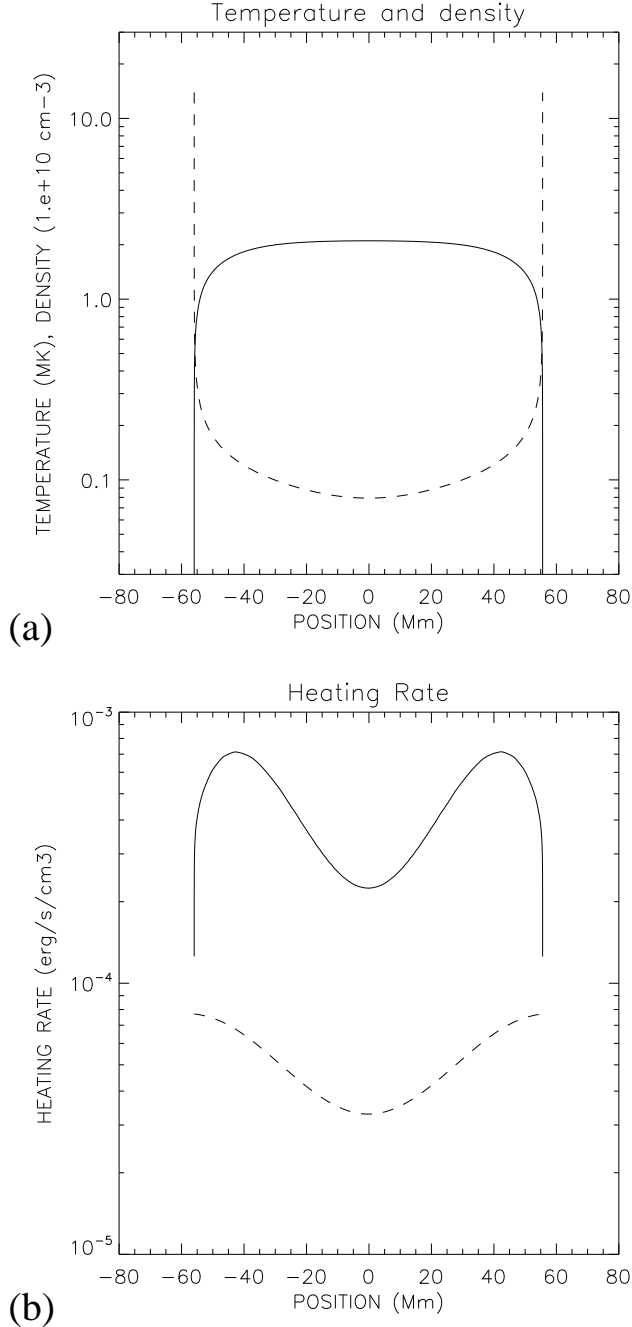


FIG. 3.— Results from modeling the energy balance of the plasma along a particular magnetic field line located at the edge of the coronal flux rope where $|\nabla\alpha_0|$ is largest. (a) Temperature $T(s)$ (*full curve*) and electron density $n_e(s)$ (*dashed curve*) as functions of position s along the field line. (b) Total heating rate $\epsilon(s)$ (*full curve*), which is a sum of hyperdiffusive heating and a “direct” contribution from photospheric footpoint motions. The latter is shown by the *dashed* curve.

the Alfvén speed $v_A(s)$ taken from the previous iteration. We assumed that the perpendicular length scale of the turbulence is characterized by $\lambda_{\text{turb}} = 10^3$ km. The chromosphere-corona transition region (TR) is assumed to be located at $z = 0$, where the temperature $T = 2 \times 10^4$ K. The solution of the energy balance equation yields the temperature $T(s)$ and electron density $n_e(s)$ as functions of position s along a field line.

Figure 3 shows modeling results for one field line at the edge of the coronal flux rope. Starting at $x = y = 0$ and $z = 43$ Mm, the field line is traced forward and backward through the

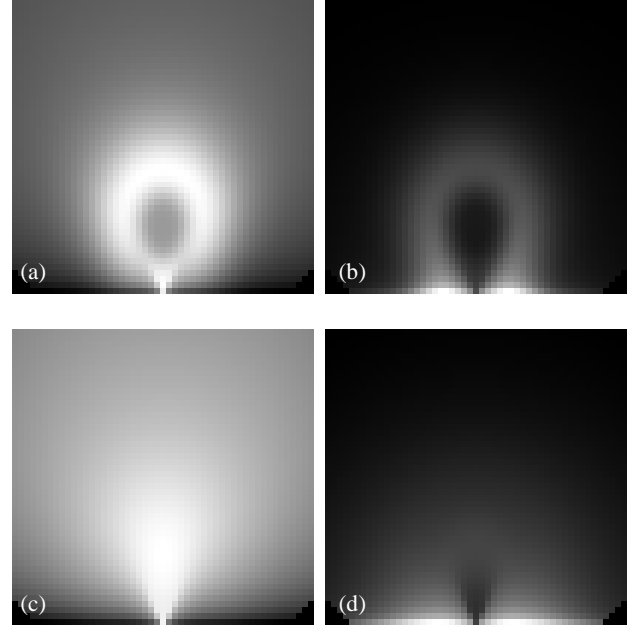


FIG. 4.— Coronal models for an active region containing a magnetic flux rope. The upper panels show results for a model with both direct and hyperdiffusive heating: (a) temperature $T(x, z)$ in a vertical plane $y = 0$ intersecting the flux rope; (b) electron density $n_e(x, z)$ in the same vertical plane. The height and width of these greyscale images correspond to 100 Mm on the Sun. The maximum temperature in the model is 2.11 MK, and the maximum density is $2.7 \times 10^9 \text{ cm}^{-3}$. The bottom panels show results for a model without hyperdiffusion: (c) temperature $T(x, z)$, and (d) electron density $n_e(x, z)$. This model has lower peak temperature and density (maximum values are 1.42 MK and $1.0 \times 10^9 \text{ cm}^{-3}$, respectively). In both models the minimum temperature is 0.37 MK, and the minimum density is $1.8 \times 10^7 \text{ cm}^{-3}$. Maximum values are shown as white; minimum values are black.

3D magnetic model until the level $z = 0$ is reached. The temperature $T(s)$ and density $n_e(s)$ along this field line are shown in Fig. 3a, and the heating rate $\epsilon(s)$ is shown in Fig. 3b (*full curve*). The dashed curve in Fig. 3b shows the “direct” contribution to the heating from photospheric footpoint motions. Note that this contribution is relatively small, so for this particular field line the heating is dominated by hyperdiffusion. However, for other field lines in the NLFFF model (e.g., along the axis of the flux rope) the hyperdiffusive heating rate is smaller than the direct heating rate.

We computed temperature and density profiles for a large number of field lines that cross the vertical plane $y = 0$. Figure 4 shows the temperature $T(x, z)$ and density $n_e(x, z)$ in the plane $y = 0$ for two different heating models. The top panels show the results when both direct and hyperdiffusive heating are applied together ($\lambda_{\text{turb}} = 10^3$ km). Note that the temperature and density are enhanced in a thick shell where the gradient of α_0 is largest. The density distribution shows a “cavity” that is round at the top and V-shaped at the bottom. The temperature is also enhanced at the bottom of the V-shaped cavity because the field lines in this region are relatively long, so the conductive cooling is reduced.

The bottom panels of Figure 4 show the temperature and density distributions in the $y = 0$ plane when only the direct heating is applied (i.e., no hyperdiffusion). The highest temperatures now occur within the flux rope where the field lines are longest and conductive losses are weakest. The lowest densities occur in the V-shaped lower part of the flux rope, but the density in the upper part is nearly the same as in the surroundings, and there is no dome-shaped cavity.

On the Sun, cavities are frequently observed in the K-corona emission, and these cavities have been linked to the presence of coronal flux ropes (see Gibson et al. 2006b, and references therein). We suggest that the observed cavities are evidence for a spatial distribution of coronal heating that is consistent with hyperdiffusion.

6. DISCUSSION AND CONCLUSIONS

We propose a new mechanism for coronal heating relevant for magnetic structures in which the large-scale magnetic field is highly sheared and/or twisted. We assume that the magnetic field in such coronal flux ropes is stochastic in nature (Lazarian & Vishniac 1999), and contains small-scale perturbations superposed on a mean magnetic field. The magnetic free energy associated with the flux rope can be converted into heat via small-scale reconnection processes. We describe this process in terms of *hyperdiffusion*, a type of magnetic diffusion in which the magnetic helicity is conserved. The effect of hyperdiffusion on the mean field depends on the gradient of the mean torsion parameter $\alpha_0(\mathbf{r}, t)$. Therefore, hyperdiffusion describes the tendency of a magnetic system to relax to a Taylor state (Taylor 1974).

In section 3 we consider helicity transport in a stochastic magnetic field, and we show that small-scale reconnection events produce a net helicity flux \mathcal{H}_0 consistent with hyperdiffusion. We derive an expression for the hyperdiffusivity η_4 in terms of the parallel and perpendicular length scales of the magnetic perturbations. The calculation is based on a simple model for the Alfvén waves produced by reconnection events (Appendix A). We find that the hyperdiffusivity depends strongly on the perpendicular length scale of the turbulence, $\eta_4 \propto \lambda_{\text{turb}}^4$. The spatially averaged heating rate ϵ_{hyper} due to hyperdiffusion is proportional to $\eta_4 |\nabla \alpha_0|^2$. This heating is distinct from the “direct” heating due to small-scale random footpoint motions. In section 4 we derive an expression for the total heating rate ϵ , which is a sum of direct and hyperdiffusive contributions.

Our analysis of the dissipation process is very approximate

and makes many simplifying assumptions. For example, we cannot identify a specific mechanism by which the stochastic magnetic field is produced and maintained. We simply treat the perpendicular length scale λ_{turb} of the fluctuating field as a free parameter to be determined from observations or more complete theories of turbulent reconnection. Also, it is unclear exactly what drives the small-scale reconnection events necessary for hyperdiffusion. The photospheric magnetic field is highly fragmented, and there are separatrix surfaces in the corona corresponding to the interfaces between photospheric flux tubes. We speculate that the reconnection events may occur at these separatrix surfaces.

In section 5 we develop a 3D model of an active region containing a magnetic flux rope, and we compute the temperature and density distributions with and without hyperdiffusion. The results show that hyperdiffusion can have a significant effect on the temperature structure, provided the perpendicular length scale of the magnetic fluctuations $\lambda_{\text{turb}} \sim 10^3$ km at the coronal base. If λ_{turb} were of order 100 km or less, the hyperdiffusive heating would not have a significant impact on the total heating rate for any field line. For the NLFFF model considered here, the heating is concentrated in a thick shell surrounding the flux rope. The heating at the axis of the flux rope is weaker, producing a “cavity” similar to the coronal cavities observed on the Sun.

At present there is no direct observational evidence to confirm or refute the existence of stochastic magnetic fields with perpendicular scales $\sim 10^3$ km. Therefore, it is unclear exactly how coronal flux ropes are heated. Coronal images obtained with the *Solar Dynamics Observatory* (SDO) may provide new observational constraints on stochastic fields and the physical processes by which coronal flux ropes are heated.

We thank Amitava Bhattacharjee for discussions about hyperdiffusion. This work was inspired by observations from Hinode/XRT. The work was supported by NASA LTSA grant NNG04GE77G, and by NASA LWS grant NNX06AG95G.

APPENDIX

TRANSPORT OF HELICITY BY ALFVÉN WAVES IN A STOCHASTIC FIELD

The transport of magnetic helicity plays an important role in the theory of hyperdiffusion. Here we consider a simple model for helicity transport due to reconnection events within the stochastic field. The average time T between reconnection events on a given flux tube is assumed to be a few times the Alfvén travel time along that tube. Let us assume that at time $t = 0$ a new section of magnetic field has just been created by reconnection. The new section connects two points P_1 and P_2 that may be located at opposite ends of a coronal loop. We neglect the loop curvature and approximate the new section as a cylindrical flux tube with radius R . We assume that in the initial state the plasma in the tube is stationary, but the torsion parameter α varies along the tube, so the field is not force free. The variable torsion causes the launch of counter-propagating Alfvén waves that travel in opposite directions along the tube. We assume that the wave length λ_{\parallel} of the waves is large compared to the tube radius. The medium surrounding the flux tube is assumed to be unaffected by the waves.

We use a cylindrical coordinate system (r, ϕ, s) where s is the distance along the tube ($0 \leq s \leq \Delta s$). The plasma is assumed to be fixed at the end points P_1 ($s = 0$) and P_2 ($s = \Delta s$), so that the waves reflect at these points. The magnetic field \mathbf{B} inside the tube is written as

$$\mathbf{B}(r, s, t) = B_0 \hat{\mathbf{s}} + \frac{r}{R} [B_{\phi,0} + \delta B_{\phi}(s, t)] \hat{\boldsymbol{\phi}}, \quad (\text{A1})$$

where B_0 is the axial field (constant in space and time), $B_{\phi,0}$ is the unperturbed azimuthal field at the cylinder wall ($r = R$), and $\delta B_{\phi}(s, t)$ is the perturbation of the azimuthal field due to the waves. The torsion parameter α is defined by $\alpha \equiv (\mathbf{B} \cdot \nabla \times \mathbf{B})/B^2$, and the perturbation of this quantity is

$$\delta \alpha(s, t) = \frac{2}{RB_0} \delta B_{\phi}(s, t). \quad (\text{A2})$$

The vector potential $\mathbf{A}(r, s, t)$ is obtained by solving the equations $\nabla \times \mathbf{A} = \mathbf{B}$ and $\nabla \cdot \mathbf{A} = 0$. Continuity with the surrounding

medium requires that $\mathbf{A}(R, s, t)$ is independent of s and t . In the limit $\lambda_{\parallel} \gg R$, the solution is given approximately by

$$\mathbf{A}(r, s, t) \approx \frac{rB_0}{2} \hat{\phi} + \frac{R^2 - r^2}{2R} [B_{\phi,0} + \delta B_{\phi}(s, t)] \hat{s}, \quad (\text{A3})$$

where $r \leq R$ and we neglect a small correction A_r needed to make $\nabla \cdot \mathbf{A}$ exactly zero. The velocity of the waves is assumed to be purely azimuthal, $\mathbf{v}(r, s, t) = (r/R)\delta v_{\phi}(s, t)\hat{\phi}$, where $\delta v_{\phi}(s, t)$ is the velocity at the cylinder wall. Inserting this expression into equation (3), we obtain the electric potential:

$$\Phi(r, s, t) \approx -\frac{R^2 - r^2}{2R} B_0 \delta v_{\phi}(s, t), \quad (\text{A4})$$

where we assumed $\eta = 0$ and required $\Phi(R, s, t) = 0$ to ensure continuity with the surrounding medium. The axial component of the helicity flux follows from equation (5):

$$\mathcal{H}_{\parallel}(r, s, t) = [\mathbf{A} \times (\mathbf{v} \times \mathbf{B} + \nabla\Phi)] \cdot \hat{s} = -\frac{r^2 B_0^2}{R} \delta v_{\phi}(s, t). \quad (\text{A5})$$

The average of \mathcal{H}_{\parallel} over the cross-section of the tube is

$$\mathcal{H}_{\parallel}(s, t) = -\frac{RB_0^2}{2} \delta v_{\phi}(s, t). \quad (\text{A6})$$

Note that the helicity flux is independent of the unperturbed azimuthal field $B_{\phi,0}$.

We now compute the helicity flux for damped Alfvén waves. In reality the damping would likely involve a turbulent cascade of wave energy to smaller spatial scales, but here we use a simple model based on an effective ‘‘frictional’’ damping. The wave equations are

$$\frac{\partial(\delta v_{\phi})}{\partial t} = \frac{B_0}{4\pi\rho_0} \frac{\partial(\delta B_{\phi})}{\partial s} - \frac{\delta v_{\phi}(s, t)}{\tau}, \quad (\text{A7})$$

$$\frac{\partial(\delta B_{\phi})}{\partial t} = B_0 \frac{\partial(\delta v_{\phi})}{\partial s}, \quad (\text{A8})$$

where ρ_0 is a constant density and τ is the frictional damping time. The boundary conditions are $\delta v_{\phi}(0, t) = \delta v_{\phi}(\Delta s, t) = 0$, which implies $\partial(\delta B_{\phi})/\partial s = 0$ at the boundaries. We assume the plasma is initially stationary, $\delta v_{\phi}(s, 0) = 0$. The initial perturbation of the torsion parameter, $\delta\alpha(s, 0)$, is assumed to be a nearly linear function of position:

$$\delta\alpha(s, 0) = -\Delta\alpha \sum_{k=0}^K \frac{4}{(2k+1)^2\pi^2} \cos\left[(2k+1)\pi\frac{s}{\Delta s}\right] \approx \Delta\alpha \left(\frac{s}{\Delta s} - \frac{1}{2}\right), \quad (\text{A9})$$

where $\Delta\alpha$ is the perturbation amplitude (we use $K = 15$). The solution of the above equations is

$$\delta v_{\phi}(s, t) = \frac{\Delta B_{\phi}}{\sqrt{4\pi\rho_0}} e^{-\gamma t} \sum_{k=0}^K \frac{4}{n^2\pi^2} \sin\left(n\pi\frac{s}{\Delta s}\right) \frac{\Omega_n}{\omega_n} \sin(\omega_n t), \quad (\text{A10})$$

$$\delta B_{\phi}(s, t) = -\Delta B_{\phi} e^{-\gamma t} \sum_{k=0}^K \frac{4}{n^2\pi^2} \cos\left(n\pi\frac{s}{\Delta s}\right) \left[\cos(\omega_n t) + \frac{\gamma}{\omega_n} \sin(\omega_n t)\right], \quad (\text{A11})$$

where $n \equiv 2k+1$; $\Delta B_{\phi} = B_0 R \Delta\alpha/2$ is the amplitude of the magnetic perturbation; $\gamma = 1/(2\tau)$ is the effective damping rate; $\omega_n = \sqrt{\Omega_n^2 - \gamma^2}$ is the mode frequency; and $\Omega_n \equiv n\pi v_A/\Delta s$ is the frequency for an undamped mode. The above solution is valid for $\gamma \leq \pi v_A/\Delta s$. The helicity flux at the mid-point of the tube ($s = \Delta s/2$) follows from equations (A6) and (A10):

$$\mathcal{H}_{\parallel}(\Delta s/2, t) = -f(t) R^2 B_0^2 v_A \Delta\alpha, \quad (\text{A12})$$

where

$$f(t) \equiv e^{-\gamma t} \sum_{k=0}^K \frac{(-1)^k}{(2k+1)^2\pi^2} \frac{\Omega_{2k+1}}{\omega_{2k+1}} \sin(\omega_{2k+1} t). \quad (\text{A13})$$

In the absence of damping ($\gamma = 0$), the helicity would oscillate back and forth between the two halves of the tube, and the time average of \mathcal{H}_{\parallel} would vanish. With damping there is a net transport of helicity from the region with high α to the region with low α :

$$\mathcal{H}_{\parallel} \approx -f_0 R^2 B_0^2 v_A \Delta\alpha, \quad (\text{A14})$$

where f_0 is the time average of $f(t)$. We assume that the next reconnection event occurs at a time T which is only a few times the Alfvén travel time, say, $T = 3\Delta s/v_A$. Then f_0 is given by a time average over the period $0 < t < T$. For a damping time τ such that $0.6 < \gamma\Delta s/v_A < \pi$, the time average of $f(t)$ is given by $f_0 \approx 0.01$. In section 3 we use the above expressions to estimate the helicity diffusivity in a stochastic field.

REFERENCES

- Acton, L., et al. 1992, *Science*, 258, 591
- Amari, T., Luciani, J. F., Aly, J. J., Mikic, Z., & Linker, J. 2003, *ApJ*, 595, 1231
- Aulanier, G., & Démoulin, P. 1998, *A&A*, 329, 1125
- Aulanier, G., Démoulin, P., & Grappin, R. 2005, *A&A*, 430, 1067
- Berger, M. A. 1984, *Geophys. and Astrophys. Fluid Dyn.*, 30, 79
- Berger, M. A., & Field, G. B. 1984, *Journal of Fluid Mech.*, 147, 133
- Berger, T., & Title, A. M. 1996, *ApJ*, 463, 365
- Berghmans, D., & Clette, F. 1999, *Sol. Phys.*, 186, 207
- Berghmans, D., McKenzie, D., & Clette, F. 2001, *A&A*, 369, 291
- Bhattacharjee, A., & Hameiri, E. 1986, *Phys. Rev. Letters*, 57, 206
- Bhattacharjee, A., & Yuan, Y. 1995, *ApJ*, 449, 739
- Blackman, E. G., & Ji, H. 2006, *MNRAS*, 369, 1837
- Bleybel, A., Amari, T., van Driel-Gesztelyi, L., & Leka, K. D. 2002, *A&A*, 395, 685
- Bobra, M., van Ballegoijen, A. A., & DeLuca, E. E. 2008, *ApJ*, in press
- Boozer, A. H. 1986, *Journal of Plasma Physics*, 35, 133
- Canfield, R. C., Hudson, H. S., & McKenzie, D. E. 1999, *Geophys. Res. Lett.*, 26, 627
- Cargill, P. J., & Klimchuk, J. A. 2004, *ApJ*, 605, 911
- Craig, I. J. D., & Sneyd, A. D. 2005, *Sol. Phys.*, 232, 41
- Cranmer, S. R., & van Ballegoijen, A. A. 2005, *ApJS*, 156, 265
- Galsgaard, K., & Nordlund, Å. 1996, *J. Geophys. Res.*, 101, 13445
- Fan, Y., & Gibson, S. E. 2007, *ApJ*, 668, 1232
- Gary, G. A., Moore, R. L., Hagyard, M. J., & Haisch, B. M. 1987, *ApJ*, 314, 782
- Gibson, S. E., et al. 2002, *ApJ*, 574, 265
- Gibson, S. E., & Fan, Y. 2006a, *J. Geophys. Res.*, 111, A12103, doi:10.1029/2006JA011871
- Gibson, S. E., & Fan, Y. 2006b, *ApJ*, 637, L65
- Gibson, S. E., Fan, Y., Török, T., & Kliem, B. 2006a, *Space Sci. Rev.*, 124, 131
- Gibson, S. E., Foster, D., Burkepile, J., de Toma, G., & Stanger, A. 2006b, *ApJ*, 641, 590
- Gudiksen, B. V., & Nordlund, Å. 2005, *ApJ*, 618, 1020
- Hagenaar, H. J., Schrijver, C. J., & Title, A. M. 1997, *ApJ*, 481, 988
- Hendrix, D. L., & van Hoven, G. 1996, *ApJ*, 467, 887
- Hendrix, D. L., van Hoven, G., Mikic, Z., & Schnack, D. D. 1996, *ApJ*, 470, 1192
- Heyvaerts, J., & Priest, E. R. 1984, *A&A*, 137, 63
- Kliem, B., Titov, V. S., Török, T. 2004, *A&A*, 413, L23
- Klimchuk, J. A., & Porter, L. J. 1995, *Nature*, 377, 131
- Kusano, K. 2005, *ApJ*, 631, 1260
- Lazarian, A., & Vishniac, E. T. 1999, *ApJ*, 517, 700
- Leka, K. D., Canfield, R. C., McClymont, A. N., & van Driel-Gesztelyi, L. 1996, *ApJ*, 462, 547
- Longcope, D. 2004, in *Proc. SOHO 15 Workshop on Coronal Heating*, St. Andrews, Scotland, 6-9 September 2004, (ESA SP-575), p. 198
- Low, B. C., & Hundhausen, J. R. 1995, *ApJ*, 443, 818
- Lu, E. T., & Hamilton, R. J. 1991, *ApJ*, 380, 89
- Magara, T., & Longcope, D. 2001, *ApJ*, 559, 55
- Mandrini, C. H., Démoulin, P., & Klimchuk, J. A. 2000, *ApJ*, 530, 999
- Manoharan, P. K., van Driel-Gesztelyi, L., Pick, M., & Démoulin, P. 1996, *ApJ*, 468, 73
- Mikić, Z., Schnack, D. D., & van Hoven, G. 1989, *ApJ*, 338, 1148
- Nisenson, P., van Ballegoijen, A. A., de Wijn, A. G., & Sütterlin, P. 2003, *ApJ*, 587, 458
- Parker, E. N. 1972, *ApJ*, 174, 499
- Parker, E. N. 1988, *ApJ*, 330, 474
- Pevtsov, A. A., Canfield, R. C., & McClymont, A. N. 1997, *ApJ*, 481, 973
- Pevtsov, A. A., Canfield, R. C., & Metcalf, T. R. 1995, *ApJ*, 440, L109
- Pevtsov, A. A. 2002, *Sol. Phys.*, 207, 111
- Porter, J. G., Fontenla, J. M., & Simnett, G. M. 1995, *ApJ*, 438, 472
- Rappazzo, A. F., Velli, M., Einaudi, G., & Dahlburg, R. B. 2007, *ApJ*, 657, L47
- Régnier, S., Amari, T., & Kersalé, E. 2002, *A&A*, 392, 1119
- Régnier, S., & Priest, E. R. 2007, *A&A*, 468, 701
- Rust, D. M., & Kumar, A. 1994, *Sol. Phys.*, 155, 69
- Rust, D. M., & Kumar, A. 1996, *ApJ*, 464, L199
- Schmieder, B., Démoulin, P., Aulanier, G., & Golub, L. 1996, *ApJ*, 476, 881
- Schrijver, C. J. 2007, *ApJ*, 662, L119
- Schrijver, C. J., DeRosa, M. L., Title, A. M., & Metcalf, T. R. 2005, *ApJ*, 628, 501
- Schrijver, C. J., & van Ballegoijen, A. A. 2005, *ApJ*, 630, 552
- Shimizu, T., Tsuneta, S., Acton, L. W., Lemen, J. R., Uchida, Y. 1992, *PASJ*, 44, L147
- Shimizu, T. 1995, *PASJ*, 47, 251
- Steenbeck, M., Krause, F., & Rädler, K. H. 1966, *Z. Naturforsch.*, 21a, 369
- Stenflo, J. O. 1989, *A&A Rev.*, 1, 3
- Sterling, A. C., Hudson, H. S., Thompson, B. J., & Zarro, D. M. 2000, *ApJ*, 532, 628
- Strauss, H. R. 1988, *ApJ*, 326, 412
- Subramanian, K., & Brandenburg, A. 2006, *ApJ*, 648, L71
- Taylor, J. B. 1974, *Phys. Rev. Lett.*, 33, 1139
- Titov, V. S., & Démoulin, P. 1999, *A&A*, 351, 707
- Török, T., Kliem, B., & Titov, V. S. 2004, *A&A*, 413, L27
- van Ballegoijen, A. A. 1985, *ApJ*, 298, 421
- van Ballegoijen, A. A. 1986, *ApJ*, 311, 1001
- van Ballegoijen, A. A. 1988, *Geophys. Astrophys. Fluid Dyn.*, 41, 181
- van Ballegoijen, A. A. 2004, *ApJ*, 612, 519
- van Ballegoijen, A. A., & Mackay, D. H. 2007, *ApJ*, 659, 1713
- Valori, G., Kliem, B., & Keppens, R. 2005, *A&A*, 433, 335
- Vishniac, E. T., & Cho, J. 2001, *ApJ*, 550, 752
- Wheatland, M. S. 2006, *Sol. Phys.*, 238, 29
- Wheatland, M. S., Sturrock, P. A., & Roumeliotis, G. 2000, *ApJ*, 540, 1150
- Wiegmann, T. 2004, *Sol. Phys.*, 219, 87